
Inflammation and Infection Imaging with a ^{99m}Tc -Neutrophil Elastase Inhibitor in Monkeys

Mary Rusckowski, Tong Qu, James Pullman, Robin Marcel, Arthur C. Ley, Robert C. Ladner, and Donald J. Hnatowich

Divisions of Nuclear Medicine and Pathology, University of Massachusetts Medical School, Worcester, Massachusetts; and Dyax Corporation, Cambridge, Massachusetts

A radiolabeled human neutrophil elastase inhibitor (EPI-HNE-2) may represent an improved nuclear medicine imaging agent for inflammation and infection. This peptide displays rapid pharmacokinetics due to its low molecular weight and localizes specifically on neutrophil elastase released in inflammatory sites by activated neutrophils. **Methods:** In this investigation, the peptide was radiolabeled with ^{99m}Tc using *N*-hydroxysuccinimidyl *S*-acetylmercaptoacetyltryglycine (NHS-MAG₃) as a bifunctional chelator and was administered on 18 occasions to 5 rhesus monkeys with inflammation/infection. **Results:** Plasma clearance was rapid, with liver and kidneys representing the major organs of accumulation. No evidence of toxicity, dosage effects, or circulating antiMAG₃-EPI-HNE-2 antibodies was observed. Specificity of localization was established using radiolabeled bovine pancreatic trypsin inhibitor (a non-hNE-binding peptide of similar size) as a nonspecific negative control peptide and by predosing with unlabeled EPI-HNE-2 to block receptor sites before the administration of radiolabeled EPI-HNE-2. The ability of radiolabeled EPI-HNE-2 to image inflammation/infection was evaluated in 12 studies in monkeys receiving only radiolabeled EPI-HNE-2 and with lesions in the arm, shoulder, or lower back. Positive images were obtained in all studies, uptake was apparent almost immediately, and images were still positive 24 h later. As a positive control, animals also received nonspecific IgG antibody radiolabeled with ^{99m}Tc either directly or by NHS-MAG₃. Compared with labeled antibody, plasma clearance of ^{99m}Tc was faster with labeled EPI-HNE-2 and accumulation in liver and heart was lower. Uptake of radioactivity in the inflammation was higher during the first hour with EPI-HNE-2 versus antibody but lower thereafter. **Conclusion:** When radiolabeled with ^{99m}Tc , EPI-HNE-2 localized specifically in inflammations in a monkey model and provided early images of diagnostic quality.

Key Words: ^{99m}Tc -peptide; inflammation and infection imaging
J Nucl Med 2000; 41:363–374

A large number of radiopharmaceuticals for inflammation and infection imaging have been considered since the observation that ^{67}Ga -citrate localizes to a useful extent in sites of inflammation (1). Roughly in chronological order, the additional imaging agents that have been used extensively in the clinic include ^{111}In -labeled mixed leukocytes

(2), ^{111}In -labeled antigranulocyte antibodies (3), and ^{111}In - and ^{99m}Tc -labeled nonspecific antibodies (4,5). At present, novel agents under investigation include ^{99m}Tc -labeled nanocolloids (6), ^{111}In -labeled chemotactic peptides (7), streptavidin and ^{111}In -labeled biotin (8), ^{99m}Tc -labeled chemotactic peptides (9), radiolabeled antibiotics (10), radiolabeled antineutrophil antibodies (11), and radiolabeled liposomes (12). Despite these considerable efforts, there remains a need for more effective radiopharmaceuticals capable of imaging acute and chronic inflammatory disease (13,14).

Many of the agents just listed are thought to localize, at least in part, by nonspecific diffusion across capillary beds damaged by microorganisms or trauma. Those radiopharmaceuticals that localize specifically at these sites (such as peptides directed against receptors expressed on activated neutrophils or antibodies with high binding affinities for bacterial determinants) may be expected to display greater specificity of localization. But those agents, such as peptides, which diffuse rapidly into inflammatory sites and clear rapidly elsewhere, may be expected to enjoy a pharmacokinetic advantage over those that accumulate and clear more slowly, such as antibodies and white cells. One potential radiopharmaceutical with properties permitting specific localization in inflammation/infection and rapid pharmacokinetics is a human neutrophil elastase inhibitor EPI-HNE-2, previously referred to as HNEI (15).

Human neutrophil elastase (hNE, E.C. 3.4.21.11, also called leukocyte elastase) is a 29-kDa protease released at high levels within neutrophils (3 pg/cell; approximately 300 $\mu\text{mol/L}$) (16). Neutrophil elastase is released into the intracellular compartment only in response to neutrophil activation by inflammatory stimuli at the site of infection/inflammation (17). Extracellular hNE, which escapes from the immediate environment of activated neutrophil, is rapidly inhibited by α -1 trypsin inhibitor (17). Using phage display technologies, a library of peptide variants based on wild-type bovine pancreatic trypsin inhibitor (BPTI) was prepared and screened against immobilized hNE. From this library, the extremely potent ($K_i = 2 \text{ pmol/L}$) and hNE-specific inhibitor EPI-HNE-2 was developed (18,19).

Neutrophil elastase has recently been considered elsewhere as a target for in vivo imaging of infection/inflammation (20). Using an alternative combinatorial approach, a DNA aptamer capable of inhibiting hNE was

Received Jan. 4, 1999; revision accepted Jun. 21, 1999.
For correspondence or reprints contact: Donald J. Hnatowich, PhD, Division of Nuclear Medicine, University of Massachusetts Medical Center, Worcester, MA 01655.

selected and, after radiolabeling with ^{99m}Tc , tested in a rat inflammation model. The localization was reported to be superior to that of radiolabeled IgG.

This laboratory has previously reported on the radiolabeling of EPI-HNE-2 and other peptides with ^{99m}Tc using *N*-hydroxysuccinimidyl *S*-acetylmercaptoacetyltriglycine (NHS-MAG₃) bifunctional chelator to attach MAG₃ to the peptide. The labeling was accomplished under mild conditions (i.e., room temperature and neutral pH). The preparation was shown to be radiochemically pure and the radiolabel was shown to be suitably stable (15).

This report describes imaging studies with ^{99m}Tc -MAG₃-EPI-HNE-2 in a nonhuman primate inflammation/infection model. Initial studies have shown that the affinity of EPI-HNE-2 for the inhibition of rat or rabbit neutrophil elastase is about 0.1 $\mu\text{mol/L}$ compared with about 1 pmol/L for human neutrophil elastase. Accordingly, a monkey model was used in this investigation in place of a rodent model. As a negative control peptide, BPTI, which differs from EPI-HNE-2 in only 8 amino acid changes at the 58 BPTI-homologous positions plus 4 additional residues at the amino terminus (added to improve expression in yeast), was radiolabeled with ^{99m}Tc in the identical manner. A total of 18 imaging studies were performed with radiolabeled peptides, 3 in which both radiolabeled BPTI and EPI-HNE-2 were administered sequentially as a test of specificity and 12 in which radiolabeled EPI-HNE-2 alone was administered. Because of the small blood volume of the monkeys, human IgG radiolabeled with ^{99m}Tc was used as a positive control in place of radiolabeled white blood cells in 2 additional studies.

MATERIALS AND METHODS

The ^{99m}Tc -pertechnetate was obtained from a ^{99}Mo - ^{99m}Tc radionuclide generator (Dupont, Billerica, MA). Four of the 5 rhesus monkeys (Michigan Biologic Products Institute, Lansing, MI), weighed between 2.4–3.0 kg, whereas the remaining monkey weighed 14 kg. IgG antibody (Sandoz, East Hanover, NJ) and other reagents (Sigma Chemical Co., St. Louis, MO) were used as received.

Radiolabeling

The synthesis of NHS-MAG₃ has been previously described (21). The methods for peptide conjugation with NHS-MAG₃ and the radiolabeling of conjugated EPI-HNE-2 and BPTI have been previously described (15). Radiolabeled antibody was administered as a positive control on 3 occasions. Direct labeling with ^{99m}Tc followed antibody reduction with 2-mercaptoethanol as previously described (22,23). The antibody was also radiolabeled with ^{99m}Tc by prior conjugation with NHS-MAG₃ as previously described (24).

EPI-HNE-2 Measurements

The equilibrium inhibition constant (K_i) and the kinetic rate constants for inhibition (k_{on} and k_{off}) have been previously reported for MAG₃-EPI-HNE-2 coupled at NHS-MAG₃:peptide molar ratios of 1:1 and 20:1 (15). These measurements were extended in this investigation to include 5:1 and 50:1 coupling along with

measurements of EPI-HNE-2 radiolabeled at pH 7.6 after coupling at 20:1.

The hNE-inhibitory activities of both coupled and mock-labeled EPI-HNE-2 samples were measured relative to unmodified EPI-HNE-2 using a room temperature fluorogenic substrate hydrolysis assay (15,18). The average number of MAG₃ groups attached per molecule was also determined using 4,4'-dithiodipyridine as previously described (15).

Preparations of *S*-acetyl-MAG₃-EPI-HNE-2 conjugated at NHS-MAG₃:EPI-HNE-2 molar ratios of 1:1, 5:1, and 20:1 were further characterized by reversed-phase high-performance liquid chromatography (HPLC) and mass spectroscopy. For each preparation, 300–500 μg peptide was loaded onto a C₁₈ reversed-phase HPLC column (YMC 345, 0.44 \times 5 cm; YMC, Inc., Wilmington, NC). Peptide bound to the column was eluted with a 0%–50% acidic (0.1% trifluoroacetic acid) water/acetonitrile gradient developed over 30 min. The absorbance at 280 nm of the column eluate was monitored with an inline ultraviolet (UV) detector, and total peptide eluting from the column was collected in 2–4 fractions. Each fraction was dried and stored frozen until reconstituted in pure water. Reconstituted HPLC fractions and samples of unmodified EPI-HNE-2 were analyzed by electrospray ionization mass spectroscopy (Mass Consortium, San Diego, CA). EPI-HNE-2 protein concentrations were determined using a 280 nm extinction coefficient of 1.1 mL/(mg/cm). Active inhibitor was determined from inhibition of calibrated hNE solutions.

Inflammation Model

All animal studies were performed with the approval of the University of Massachusetts Medical Center Institutional Animal Care and Use Committee. A literature search provided little guidance in the development of an inflammation/infection model in primates. The model described herein was developed during the course of this investigation in 18 studies involving 5 animals and several ^{99m}Tc -labeled peptides and proteins.

In the earliest 3 studies, a sterile inflammation was induced by subcutaneous injection of a mixture of zymosan A (from *Saccharomyces cerevisiae*, Sigma) and arachidonic acid (Sigma) (25–27). In most of the remaining studies, inflammation was induced by the subcutaneous administration of heat-killed *Staphylococcus aureus* (Sigma) along with arachidonic acid. The injectates were prepared under sterile conditions by suspending 15 mg dried *S. aureus* cell product in 1 mL sterile saline with mixing and sonication. An ampule containing 50 mg arachidonic acid was mixed into a uniform suspension with 0.15 mL sterile saline by continuous pipette action. The entire 0.15 mL was added to 0.4 mL of the cell suspension for injection.

Four studies used infectious lesions in which live *S. aureus* was added to the injectate. An isolated colony (#29213; American Type Culture Collection, Rockville, MD) grown on beef agar was transferred to yeast-peptone broth and incubated at 37°C for 4–6 h. Of this culture, 10 or 100 μL mixed with the sterile injectate were administered.

Before injection to establish an inflammation, the animal was anesthetized by intramuscular injection of 20 mg/kg ketamine (Fort Dodge Laboratories, Inc., Fort Dodge, IA). The target area was shaved, swabbed with alcohol, and the mixture of arachidonic acid with *S. aureus* was administered subcutaneously. The sites of inflammation included the left upper arm (3 studies), the dorsal left shoulder (5 studies), the lower back (8 studies), and the thigh (1

study). The radiolabeled peptides and radiolabeled antibody were administered 1–4 d after induction of the inflammation.

Imaging Protocol

Scintigrams were acquired using a portable large-field-of-view scintillation camera (Elscont, Hackensack, NJ) equipped with a parallel-hole, medium-energy collimator and an Elscint APEX F1 computer. Images were acquired for a present time of 30–480 s using a 256×256 matrix with a 20% energy window set at 140 keV.

For radioactivity administration and imaging, each animal was anesthetized with ketamine and was positioned posteriorly on the collimator face. To maintain anesthesia, the animal was intubated with an uncuffed tracheal tube (Mallinckrodt, Inc., St. Louis, MO) and given 2% isoflurane (Abbott Labs, N. Chicago, IL) in oxygen.

An inline catheter was placed into a vein on the right arm through which the radioactivity was administered as an intravenous bolus. About 10 min after the administration and throughout the imaging period, lactated Ringers solution (Baxter Health Care, Deerfield, IL) was infused through the catheter at a rate of about 24 mL/h to maintain electrolytic balance. The animals received dosages between 1 and 100 μg radiolabeled peptide at specific activities between 0.4 and 15 MBq. The radiolabeled antibodies were administered at dosages of 41 and 44 μg (22 MBq; direct) and 49 μg (44 MBq; MAG_3 -coupled). Animals were typically imaged for periods of 30–480 s at various times during the first day and for periods of up to 45 min on the following day.

During analysis of the whole-body images, regions of interest (ROIs) were placed about the left and right kidneys, the heart, the liver, the lesion (target arm/shoulder/lower back), and contralateral regions of each image, and the counts were recorded without absorption correction. An estimate of the radioactivity in microcuries within each region was obtained by applying the counts to a calibration curve of counts per minute (cpm) versus microcuries. Results were then normalized to the radioactivity administered.

In a test of specificity, 1 animal was imaged on 2 separate occasions separated by 2 wk. Radiolabeled BPTI was administered first, followed by radiolabeled EPI-HNE-2. The animal received the same dosage of radiolabeled peptides (25, 22 MBq on 24, 27 μg with BPTI or EPI-HNE-2, respectively). In both cases, on the day previous to imaging, the animal received the same volume of sterile *S. aureus*/arachidonic acid injectate in the identical location within the lower back.

In a second test of specificity, a large excess of unlabeled, unmodified EPI-HNE-2 was administered to block peptide-specific binding sites before the administration of $^{99\text{m}}\text{Tc}$ - MAG_3 -EPI-HNE-2. Two experiments, using different animals with inflammations induced in the lower back, were performed. One animal received 2.1 mg unlabeled peptide 45 min before receiving the radiolabeled peptide, whereas the other animal received 4.5 mg 1.5 h earlier. The latter animal also received 40 μg IgG antibody radiolabeled directly with $^{99\text{m}}\text{Tc}$ 3 h after the administration of the radiolabeled EPI-HNE-2. The IgG was used to verify the presence of the lesion.

Sample Collection

Blood samples (each about 0.2 mL) were obtained by needle stick. Each was collected in an ethylenediamine tetraacetic acid vacutainer and immediately placed on ice for plasma analysis. Samples were counted for radioactivity against a standard of the injection so that the results could be presented as a percentage

injected dosage (%ID) per milliliter of plasma. Whenever possible, urine samples were collected directly into sterile tubes by depressing the animal's bladder. Samples of plasma and urine were also analyzed by size-exclusion HPLC. Samples not analyzed immediately were stored at 4°C.

To determine the percentage of radiolabel added, which became bound to formed elements, radiolabeled EPI-HNE-2 was added to fresh whole blood to a concentration of 2 $\mu\text{g}/\text{mL}$ in heparin tubes and incubated at 37°C for 1 h. The formed elements were then pelleted by centrifugation, rinsed with cold 0.1 mol/L phosphate-buffered saline, and counted in a NaI(Tl) well counter.

Anti-EPI-HNE-2 Assay

Two primates each received as many as 6 administrations each of 10–100 μg MAG_3 -EPI-HNE-2, over a 12-mo period. An assay, based on immobilized Protein A/G gel (Pierce, Rockford, IL), was developed to detect anti MAG_3 -EPI-HNE-2 antibodies in plasma from these animals. A 3-mL column of gel (1.5×1.0 cm) was equilibrated with 15 mL binding buffer (Pierce). The plasma sample under investigation was diluted 1:1 with binding buffer, and 0.1 mL of this solution was applied to the column and was washed through with an additional 15 mL binding buffer. To detect if the column-bound plasma antibodies contained anti- MAG_3 -EPI-HNE-2 activity, 1 μg radiolabeled EPI-HNE-2 was added to the column and was washed through with about 40 mL binding buffer. Any bound radioactivity was then eluted with 15 mL elution buffer (Pierce) and collected for counting. Nonspecific binding was shown to be minimal by the addition of radiolabeled EPI-HNE-2 without the prior plasma addition. Plasma obtained from one animal that had not yet received EPI-HNE-2 was used as a negative control.

Antibodies to the EPI-HNE-2 peptide were generated in a rabbit (New Zealand White; Milbrook Farms, Amherst, MA) for use in validating the assay. Briefly, the rabbit was inoculated with 100 μg peptide in adjuvant (TiterMax Classic, Sigma), boosted with an additional 100 μg in incomplete Freund's adjuvant 2 wk later, and, finally, after 3 wk was boosted again with 100 μg in saline alone. Two weeks later, 15 mL whole blood was obtained from an ear vein. After centrifugation, the serum was purified on a 3-mL column of Immopure Immobilized Protein A/G (Pierce) in 3 batches of 2.5–3 mL each. The immunoglobulin fraction was pooled and dialyzed against saline for 2 d at 4°C with 4 changes. The IgG was aliquoted and stored at -20°C .

RESULTS

Radiolabeling

After P-4 purification, radiochemical purity by Sep-Pak analysis averaged 91% (3% SD, $n = 19$) for radiolabeled EPI-HNE-2 and 90% (3% range, $n = 3$) for radiolabeled BPTI (15). The radiochemical purity of the radiolabeled antibody was $>95\%$ (24), the radioactivity profile matched the UV profile, and HPLC recoveries averaged 85%.

Characterization of MAG_3 -EPI-HNE-2

Unmodified EPI-HNE-2 contains 3 potential sites for reaction with NHS- MAG_3 : the ϵ -amino groups of 2 lysine residues and the amino terminus. The data in Table 1 show that the average number of *S*-acetyl- MAG_3 groups per EPI-HNE-2 molecule, measured using 4,4'-dithiodipyridine (15), increases with increasing NHS-*S*-acetyl- MAG_3 :EPI-

TABLE 1
Properties of MAG₃-EPI-HNE-2 Coupled at Different MAG₃:EPI-HNE-2 Molar Ratios

Coupling ratio MAG ₃ :EPI-HNE-2	Average groups per molecule	Observed mass peaks* (Da)	Active inhibitor (%)	K _i (pmol/L)	k _{on} (10 ⁶ /mol/L/s)	k _{off} (10 ⁻⁶ /s)
Native, unmodified	0	<u>6753</u>	100	1.2	4.7	5.8
1:1	0.05†	<u>6753</u> , <u>7041</u>	112	0.7	6.0	4.0
5:1	1.5‡	<u>6753</u> , <u>7042</u> <u>7327</u> , <u>7614</u>	96	0.7	6.8	4.6
20:1	2.2‡	<u>7353</u> , <u>7660</u>	108	ND	ND	ND
50:1	ND	ND	90	1.1	5.2	5.7
20:1, mock radiolabeled	ND	ND	108	1.7	6.1	10.0

*The major mass peak in each sample is underlined.
†Average (n = 3, single preparation).
‡Average (n = 6, two preparations).
ND = not determined.

HNE-2 coupling ratio. *S*-acetyl-MAG₃ per EPI-HNE-2 increases from 0.05 at a NHS-*S*-acetyl-MAG₃:EPI-HNE-2 coupling ratio of 1:1 to more than 2 at a coupling ratio of 20:1.

Mass spectrometric analysis of HPLC-purified preparations of unmodified EPI-HNE-2 and *S*-acetyl-MAG₃-EPI-HNE-2 confirms the addition of *S*-acetyl-MAG₃ groups to EPI-HNE-2 after coupling (Table 1). Unmodified EPI-HNE-2 shows a single major mass peak at the expected molecular weight of the unmodified peptide: 6753 Da. (The major mass peak in each sample is underlined in Table 1.) When NHS-MAG₃ is coupled to EPI-HNE-2 at a 1:1 molar ratio, a second mass peak, at 7041 Da, is obtained in addition to the main mass peak at 6753 Da. The mass spectrum of *S*-acetyl-MAG₃-EPI-HNE-2 coupled at a 5:1 molar ratio shows the major mass peak is now at 7041 Da, along with 3 lower-intensity mass peaks. The solubility of *S*-acetyl-MAG₃-EPI-HNE-2 coupled at a 20:1 molar ratio is low after HPLC purification. Only 30% of the material applied to the HPLC column was soluble after drying the HPLC column eluate. The mass spectrum of this material showed 2 mass peaks of approximately equal intensity.

A mass of 7041 Da is consistent with the addition of a single *S*-acetyl-MAG₃ group (288 Da) to the otherwise unmodified EPI-HNE-2 molecule. Additions of 2 and 3 *S*-acetyl-MAG₃ groups per EPI-HNE-2 would produce molecules of mass 7329 and 7617 Da, respectively. We conclude from the data in Table 1 that the reaction of EPI-HNE-2 with NHS-*S*-acetyl-MAG₃ results in the addition of *S*-acetyl-MAG₃ groups to the peptide and that the number of *S*-acetyl-MAG₃ groups added per peptide increases with the NHS-*S*-acetyl-MAG₃-to-peptide ratio with up to 3 *S*-acetyl-MAG₃ groups attached at high ratios. The interaction of EPI-HNE-2 with hNE is not significantly affected either by the attachment of multiple MAG₃ groups to the molecule or by the chemistry used to incorporate ^{99m}Tc into *S*-acetyl-MAG₃-EPI-HNE-2. Table 1 also presents results of EPI-HNE-2 characterizations after NHS-MAG₃ coupling and, in

one case, mock radiolabeling. Some values within Table 1 have been reported previously (15). The percent active inhibitor (measured as hNE inhibition activity per unit A₂₈₀), equilibrium inhibition constant (K_i), and kinetic rate constants (k_{on} and k_{off}) are invariant, within the accuracy of the measurements, for all of the conditions listed.

Inflammation/Infection Model

In all cases, a visible swelling was apparent at or near the injection site approximately 24 h after induction of the inflammation. The inflammation spontaneously resolved over the next several days in all cases except for the 1 animal receiving the highest dosage of live *S. aureus*. In that case, the site became inflamed, but resolved after a course of antibiotics. On several occasions, the lesion was biopsied. A pus-like exudate was smeared and stained with Wright-Giesma stain. Examination of a histological section showed massive infiltration of neutrophils.

Pharmacokinetics

When incubated with whole blood, only 2.1% ± 0.8% (n = 3) of ^{99m}Tc-MAG₃-EPI-HNE-2 localized on formed elements after 1 h incubation at 37°C. Thus, under the conditions of the in vitro incubation, binding of the radiolabel to formed elements was essentially negligible.

Figure 1 presents size-exclusion HPLC radiochromatograms of ^{99m}Tc-MAG₃-EPI-HNE-2 before administration (Fig. 1A) and of plasma collected at 15 min (Fig. 1B) and urine collected at 6.5 h (Fig. 1D) postadministration. This figure was obtained after administration of 28 μg (2226 μCi) of ^{99m}Tc-MAG₃-EPI-HNE-2 to an animal that had received radiolabeled EPI-HNE-2 on a total of 5 previous occasions over 11 mo. For both blood and urine samples, the major radioactivity peak elutes from the column at the same position (fraction 40) as ^{99m}Tc-MAG₃-EPI-HNE-2. In the plasma sample, radioactivity associated with the radiolabeled peptide peak accounts for more than 90% of the counts eluting from the column. In contrast, the radiolabeled peptide peak in the urine sample contains little more than

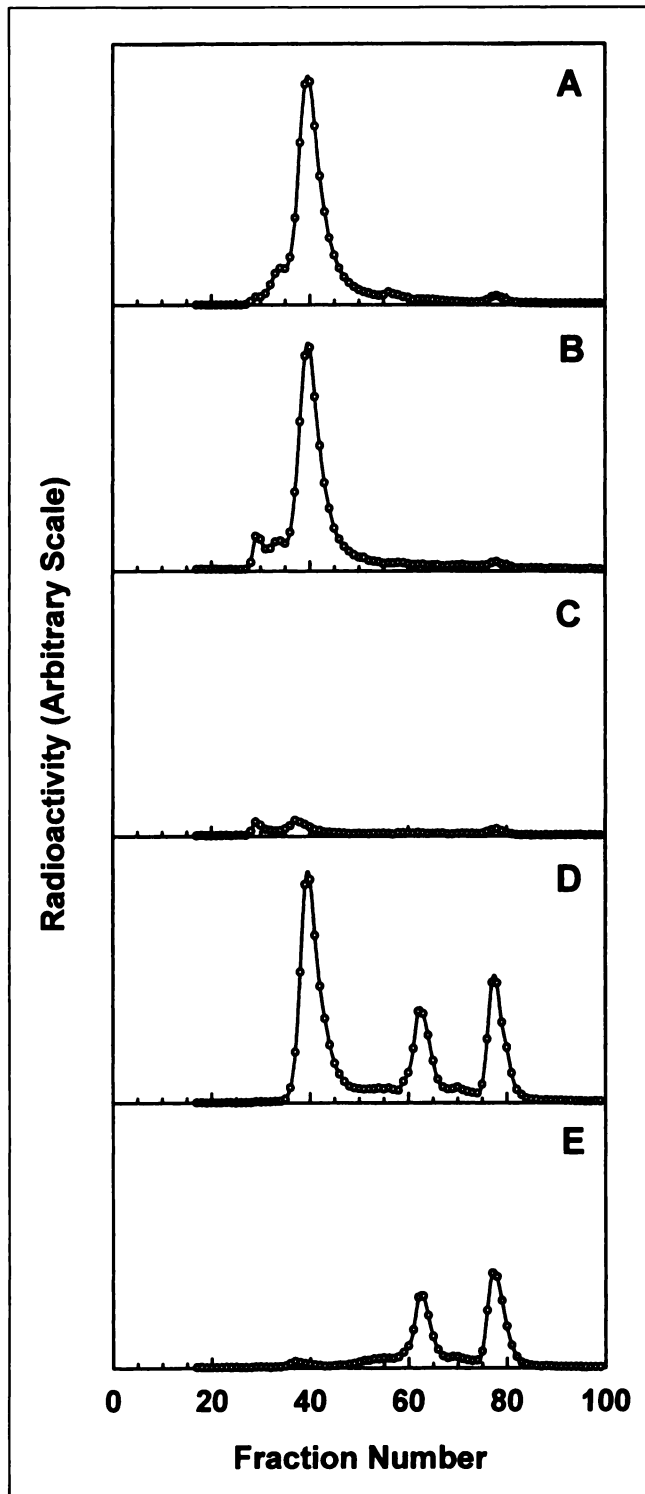


FIGURE 1. Size-exclusion HPLC radiochromatographic profiles of ^{99m}Tc -MAG₃-EPI-HNE-2 before administration (A); for plasma collected at 15 min (B); and for urine collected at 6.5 h (D) postadministration. The figure also shows the radiochromatograms obtained after incubation with hNE-immobilized beads to remove radioactivity bound to EPI-HNE-2 in plasma (C) and in urine (E).

half of the total counts eluting from the column. The majority of the remaining counts elute in 2 apparent low-molecular-weight peaks at fractions 65 and 78. The species eluting in fractions 65 and 78 in the urine analysis have previously been identified as radiolabeled cysteine resulting from the transchelation of the label *in vivo* from peptide to endogenous cysteine (23,28).

Aliquots of the plasma and urine samples were incubated with a molar excess of hNE immobilized on agarose beads to remove ^{99m}Tc -MAG₃-EPI-HNE-2. Figure 1 shows the radiochromatograms obtained after these incubations of plasma (Fig. 1C) and urine (Fig. 1E). Nearly complete loss of the main peak from both plasma and urine after addition of the beads identifies the species responsible in both as ^{99m}Tc -MAG₃-EPI-HNE-2. The peaks attributed to cysteine are not removed from urine by the incubation with hNE-immobilized beads.

Figure 2 shows representative plasma clearance on a semilog scale of radioactivity (%ID/mL) separately for 4 animals that received ^{99m}Tc -MAG₃-EPI-HNE-2 alone (i.e., without the prior administration of radiolabeled BPTI; closed symbols). For comparison, Figure 2 also shows plasma clearance after 2 administrations of radiolabeled antibody (open symbols). Clearance of labeled EPI-HNE-2 appeared to be independent of the animal and EPI-HNE-2 dosage administered (data not presented). Each clearance curve was analyzed separately to obtain the clearance half-times (29). The clearance curve of labeled peptide is biphasic, with average half-lives of 7.3 min ($t_{1/2\alpha}$, SD 2.9 min, $n = 6$; intercept, $68\% \pm 9\%$) and 244 min ($t_{1/2\beta}$, SD 126 min, $n = 6$). As expected, plasma clearance is much slower after administration of the radiolabeled antibody and is essentially unchanged over the 4-h collection period.

Figure 3A presents the counts (in %ID/pixel) in liver, heart, both kidneys, and lesion over 4 h for 1 representative study using ^{99m}Tc -MAG₃-EPI-HNE-2 (closed circles) and 1 study using radiolabeled IgG (open circles). The rapid clearance of ^{99m}Tc -MAG₃-EPI-HNE-2 from plasma is reflected in the low and rapidly decreasing levels of radioactivity in the heart (primarily blood pool) relative to that of ^{99m}Tc -labeled IgG. Accumulation of radioactivity in the liver is higher for ^{99m}Tc -IgG than for ^{99m}Tc -MAG₃-EPI-HNE-2, whereas in the kidneys this situation is reversed. The differences in accumulation in these 2 organs may reflect different routes of clearance from circulation for large molecules such as IgG (hepatobiliary) and peptides (renal).

The kinetics of radioactivity accumulation in the lesion are different for the 2 agents. After administration of labeled peptide, counts rapidly accumulate to a maximum level, reached about 30 min postadministration, which is maintained unchanged throughout the remainder of the 4-h imaging period. In contrast, administration of ^{99m}Tc -labeled IgG results in a slower accumulation of counts at the lesion site throughout the entire imaging period.

Figure 3B presents ratios of radioactivity in the lesion to that in liver, heart, kidneys, and contralateral site for a representative study of radiolabeled EPI-HNE-2 (closed

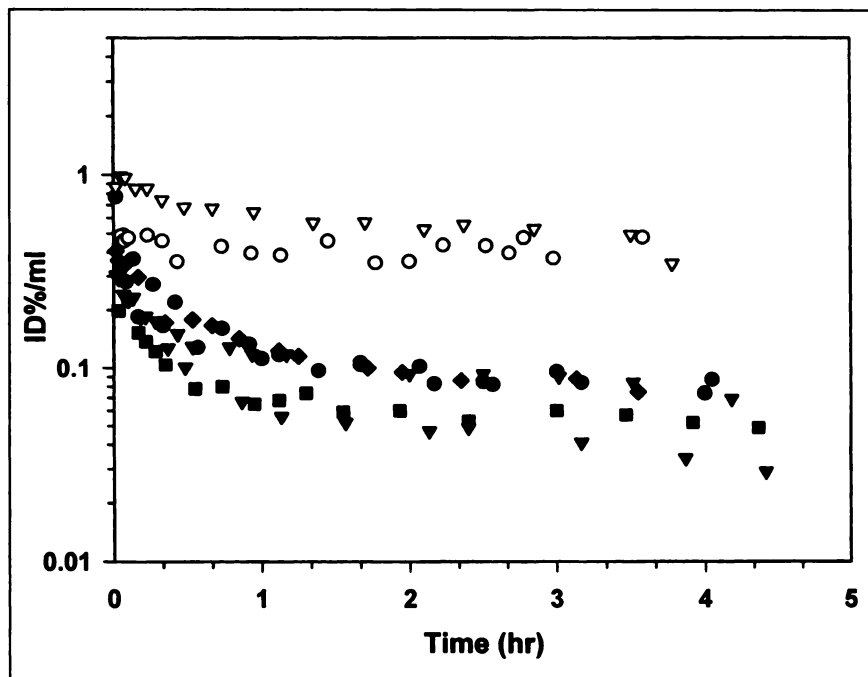


FIGURE 2. Plasma clearance of radioactivity (in %ID/mL) over 4 h for representative 4 animals receiving radiolabeled EPI-HNE-2 alone (closed symbols) and 2 animals receiving radiolabeled antibody (open symbols), normalized to same injected activity.

circles) and 1 study of radiolabeled antibody (open circles). Radioactivity (in %ID/pixel) in whole liver, heart, and both kidneys was compared with radioactivity in an ROI within the lesion. The same size region was used for both peptide and antibody and both contralateral sites. The target-to-organ ratios after administration of labeled antibody are lower because of higher radioactivity levels in these organs for labeled antibody. Also, because of the higher radioactivity levels in kidneys after administration of labeled EPI-HNE-2, the ratio of radioactivity in the lesion to that in kidneys is lower after the first hour for labeled EPI-HNE-2. The ratio of lesion-to-contralateral site is similar for both carriers at all time points.

Absence of Immune Response

To validate the Protein A/G column assay, we performed control studies using the pooled rabbit anti-EPI-HNE-2 antibody solution (positive control) or serum from a monkey who had not yet received EPI-HNE-2 (negative control). The test solutions were applied to the Protein A/G column as described earlier for plasma samples. Addition of the negative control serum resulted in only a few percent of radiolabeled EPI-HNE-2 binding to the column, whereas 70% of the radioactivity bound after addition of the anti-EPI-HNE-2 antibody.

Using this assay, no evidence was obtained for the presence of anti-MAG₃-EPI-HNE-2 antibodies in plasma samples taken from 2 monkeys administered labeled EPI-HNE-2 on 5 occasions each over 11 mo. The absence of anti-MAG₃-EPI-HNE-2 antibodies in circulation may also be indicated by the absence of a pronounced high molecular weight peak on HPLC analysis of plasma samples (Fig. 1). Further, liver radioactivity levels did not increase with subsequent administrations of radiolabeled EPI-HNE-2, as

would have been expected in the presence of anti-MAG₃-EPI-HNE-2 antibodies (data not presented).

Whole-Body Images

BPTI, a peptide of similar size and structure to EPI-HNE-2, has no affinity for hNE (18,19). Therefore, ^{99m}Tc-MAG₃-BPTI can be used to establish the level of nonspecific accumulation at the inflammatory locus of small radiolabeled peptides of similar size and structure, such as EPI-HNE-2. Figure 4 presents whole-body images obtained from an experiment to compare the extents of accumulation at the site of a sterile inflammation of radiolabeled BPTI and EPI-HNE-2. The same animal was imaged on 2 separate occasions separated by 2 wk, after having received radiolabeled BPTI and then radiolabeled EPI-HNE-2. No obvious differences were evident on visual inspections of the resulting lesions. However, the image of the lesion in the lower back was more pronounced after administration of radiolabeled EPI-HNE-2.

In a second test of specificity, a large excess of unlabeled, unmodified EPI-HNE-2 was administered to block peptide-specific binding sites before the administration of ^{99m}Tc-MAG₃-EPI-HNE-2. Two experiments, using different animals with inflammations induced in the lower back, were performed. One animal received unlabeled peptide 45 min before receiving the radiolabeled peptide, whereas the other animal received the unlabeled peptide 1.5 h earlier. The latter animal also received ^{99m}Tc-labeled IgG antibody 3 h after the administration of the radiolabeled EPI-HNE-2. The IgG was used to verify the presence of the lesion.

Figure 5 is a composite showing the 1-h whole-body images of both animals who received the unlabeled EPI-HNE-2 (Figs. 5A and B) and the 1-h whole-body image of the animal receiving the radiolabeled antibody 4 h after

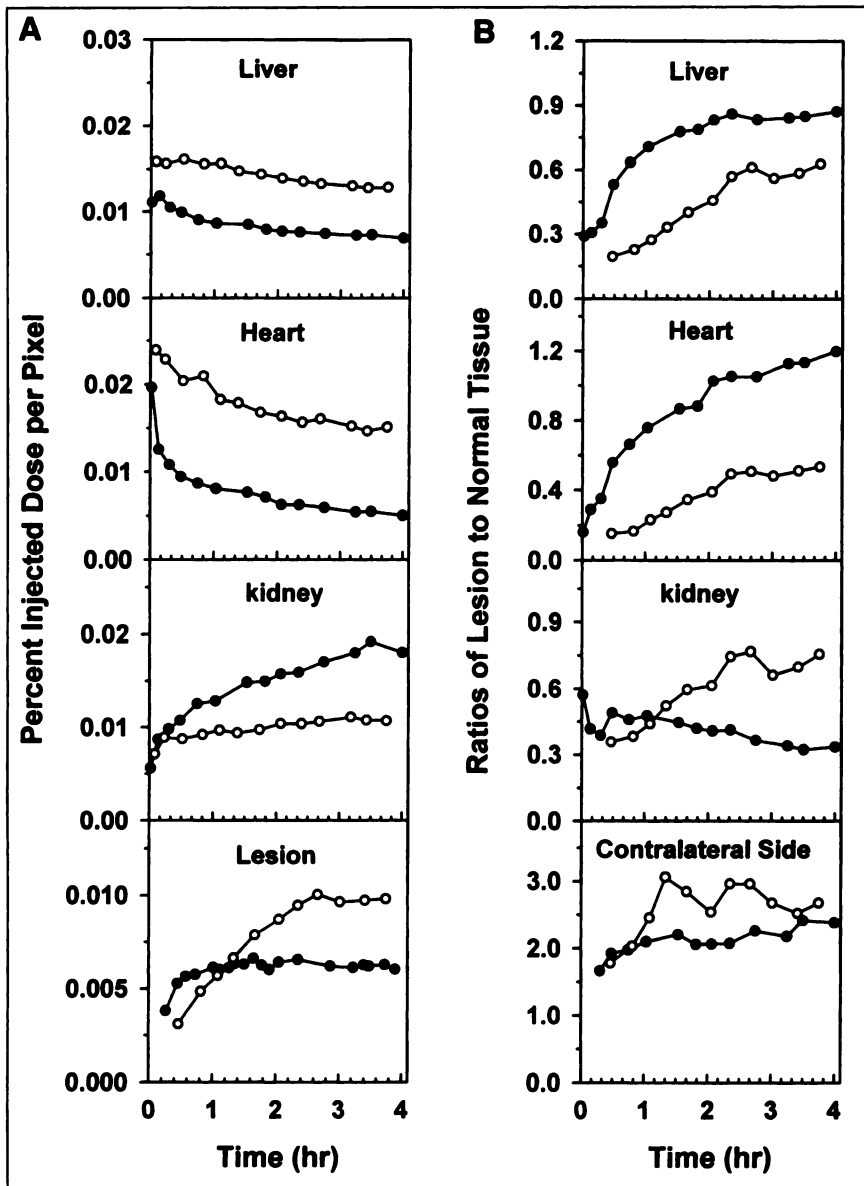


FIGURE 3. (A) Comparison of radioactivity levels (in %ID/pixel) over 4 h in liver, heart, both kidneys, and in lesion for 1 representative animal receiving radiolabeled EPI-HNE-2 alone (●) and 1 representative animal receiving radiolabeled antibody (○). (B) Ratios of lesion to liver, heart, kidney, and contralateral site for representative study of radiolabeled EPI-HNE-2 alone (●) and 1 study of radiolabeled antibody (○).

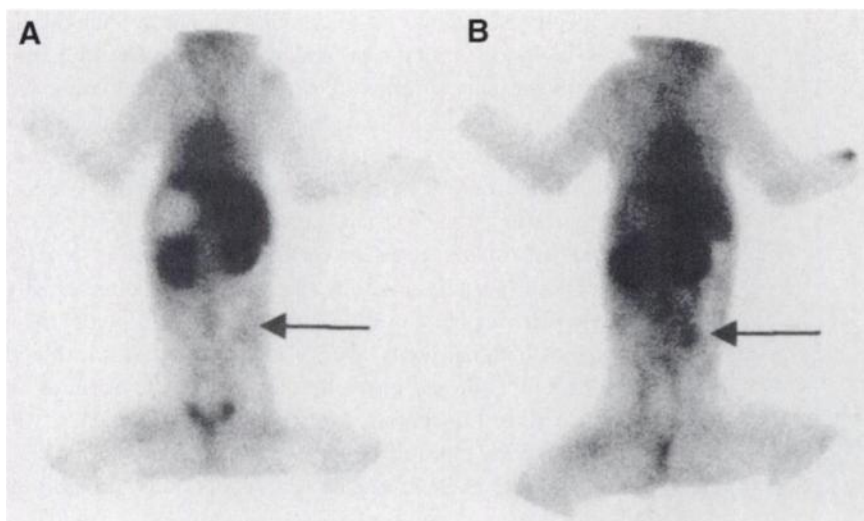


FIGURE 4. Whole-body images obtained 2 h after administration of radiolabeled BPTI control (A) and 2 h after administration of radiolabeled EPI-HNE-2 (B) separated by 2 wk in same animal with reproducible inflammation in lower back. Increased accumulation of radioactivity at site of inflammation (B) indicates specific binding of ^{99m}Tc -MAG₃-EPI-HNE-2 therein.

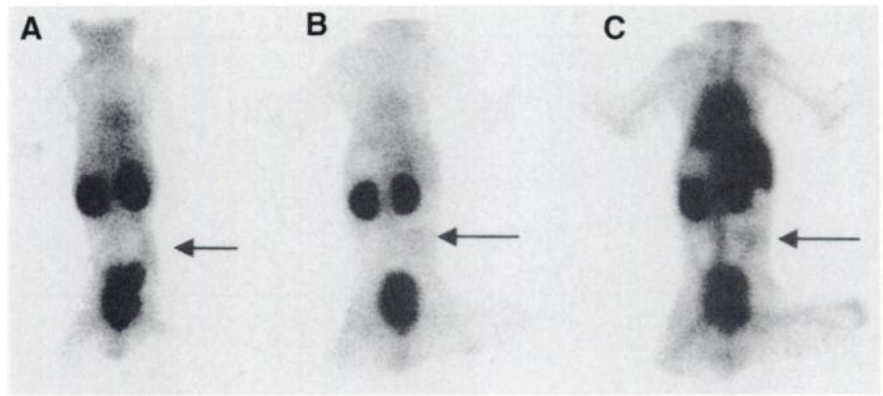


FIGURE 5. Whole-body images at 1 h postadministration of radiolabeled EPI-HNE-2 in 2 animals receiving unlabeled EPI-HNE-2 45 min (A) and 1.5 h (B) earlier. Also shown is whole-body image at 1 h postadministration of radiolabeled IgG for comparison (C). Inflammation (arrow) is readily apparent only in IgG image.

receiving the labeled peptide (Fig. 5C). The inflammation in the lower back (arrow) is apparent in the IgG image along with high levels of radioactivity in heart, vasculature, kidneys, vertebra, bladder, and liver as expected. By contrast, the 2 animals pre-dosed with EPI-HNE-2 show only faint radioactivity accumulation everywhere except in kidneys, gallbladder, and bladder. In particular, the inflammation site is barely evident, in contrast to images obtained without the blocking peptide. In addition, both images show much less background radioactivity than that seen in all animals receiving the radiolabeled EPI-HNE-2 alone. This result suggests that there may be specific receptors for EPI-HNE-2 in normal organs and/or activated neutrophils diffused from the lesion site.

Figure 6 presents the percentage of the injected radioactivity localized in the lesion versus time for both animals receiving the blocking peptide and for 1 representative animal receiving about the same dosage of radiolabeled EPI-HNE-2 (24 versus 15 and 21 μg) but without the blocking peptide. The accumulation of radioactivity in the

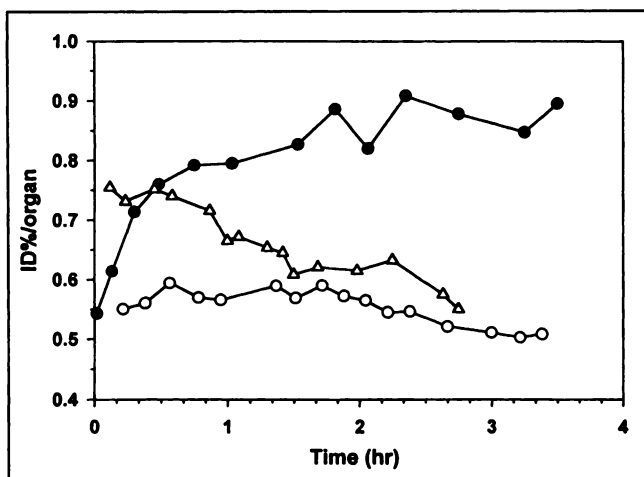


FIGURE 6. Percentage of $^{99\text{m}}\text{Tc}$ in inflammation versus time for the 2 animals receiving blocking peptide (○ and △) in comparison with 1 representative animal not receiving blocking peptide (●).

lesion is lower at all but the earliest time points in animals receiving the blocking peptide and is similar to the levels obtained using radiolabeled BPTI.

Radiolabeled IgG or white blood cells are currently the agents of choice in the clinic for imaging sites of inflammation/infection. Because of the small blood volume of the monkeys, in this study, human IgG radiolabeled with $^{99\text{m}}\text{Tc}$ was used in place of radiolabeled white blood cells as a positive control to validate the primate model and to serve as a reference for comparison. The results obtained with direct-labeled and MAG_3 -coupled IgG were sufficiently similar that the pharmacokinetics were averaged. Figure 7 presents a series of whole-body images obtained in the first 4 h postadministration of 44 μg direct-labeled IgG. Indications of the sterile lesion in the lower left quadrant (arrow) are evident in the earliest image at 28 min as 2 separate hot spots. Thereafter, activity within the lesion becomes more distinct before beginning to fade at 4 h. In this study, the lesion was still evident at 24 h. Along with activity in the lesion, radioactivity in the heart, vasculature, kidneys, vertebra, bladder, and, especially, the liver are evident throughout the counting period.

Twelve of the 18 studies were of $^{99\text{m}}\text{Tc}$ - MAG_3 -EPI-HNE-2 alone. Despite a large range of dosages (0.9–95 μg) and specific activities (11–400 mCi/mg), no obvious differences in biodistribution or image quality were apparent. Figure 8 presents a series of whole-body images obtained during the first 4 h postadministration of radiolabeled EPI-HNE-2. The gray scales of this and the previous figure are identical. Radioactivity in the sterile inflammatory lesion in the lower left quadrant (arrow) exceeds that of the contralateral side even in the earliest image. However, at 75 min, and especially at 2 h, the inflammation is readily evident. The lesion was still evident at 24 h. In comparison to images obtained with labeled antibody, activity in blood pool, in the liver, and in the vertebra are less evident at all but the earliest time points. More apparent is radioactivity in the gallbladder, possibly in facial mucosa, and what appear to be slight uptakes throughout the whole body, possibly in muscle.

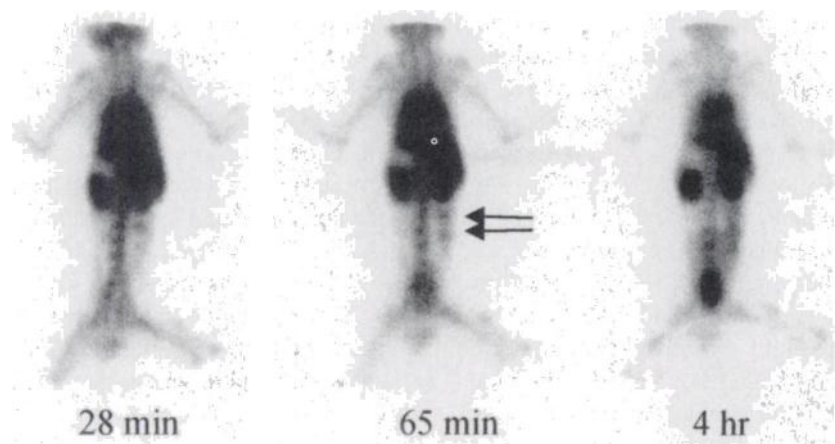


FIGURE 7. Series of whole-body images obtained between 28 min and 4 h postadministration of radiolabeled IgG show radioactivity accumulations in liver, heart, vasculature, kidneys, vertebra bladder, and nonsterile inflammatory lesion (arrows).

DISCUSSION

A large number of radiopharmaceuticals, both experimental and established, are presently used for inflammation/infection imaging (13,14). In general, the mechanism of localization is, at least in part, associated with nonspecific diffusion across leaky capillaries. It seems evident that radiopharmaceuticals localizing specifically in inflammation will exhibit superior specificity and, therefore, should be superior agents. Furthermore, the majority of all radiopharmaceuticals for inflammation imaging tend to display slow pharmacokinetics, usually because they depend on radiolabeled cells or large molecules to carry the radiolabel. It may also seem evident that agents with rapid pharmacokinetics may be preferable (especially when radiolabeled with ^{99m}Tc because of its short 6-h physical half-life), because they may permit earlier diagnosis.

Thus, certain ^{99m}Tc-radiolabeled peptides may eventually become the radiopharmaceuticals of choice, at least in acute inflammatory diseases. The chemotactic peptides, for example, are thought to bind specifically to activated neutrophils at the inflammatory site (30). Furthermore, as small peptides, they have been shown to clear rapidly as expected (31). However, a disadvantage of the chemotactic peptides is

their toxicity (32). In this report, we describe the radiolabeling and use of a novel peptide inhibitor of human neutrophil elastase, EPI-HNE-2, as an agent for in vivo imaging of inflammatory sites.

All inflammatory conditions are accompanied by infiltration of large numbers of neutrophils. The azurophil granules within the neutrophil are rich in proteases, the most abundant of which, hNE, is present at concentrations estimated at about 300 μmol/L within the cell, or about 3 pg per cell (33). Neutrophil elastase is a highly cationic protein and is thought to be retained at inflammatory sites by binding to highly anionic surfaces of cells. However, hNE that diffuses from the inflammation will be rapidly and irreversibly bound to and inhibited by α-1-protease inhibitor, the principal endogenous inhibitor of hNE in blood (34). Free hNE is therefore only present at the site of inflammation and, as a specific marker for the presence of activated neutrophils, should be a potentially ideal molecular target for imaging foci of inflammation/infection.

Using phage display technologies, variants of the low molecular weight protease inhibitor peptide BPTI (mol wt = 6512 Da) have been obtained that have very high affinity for hNE (about 1 pmol/L) and very low affinities for other

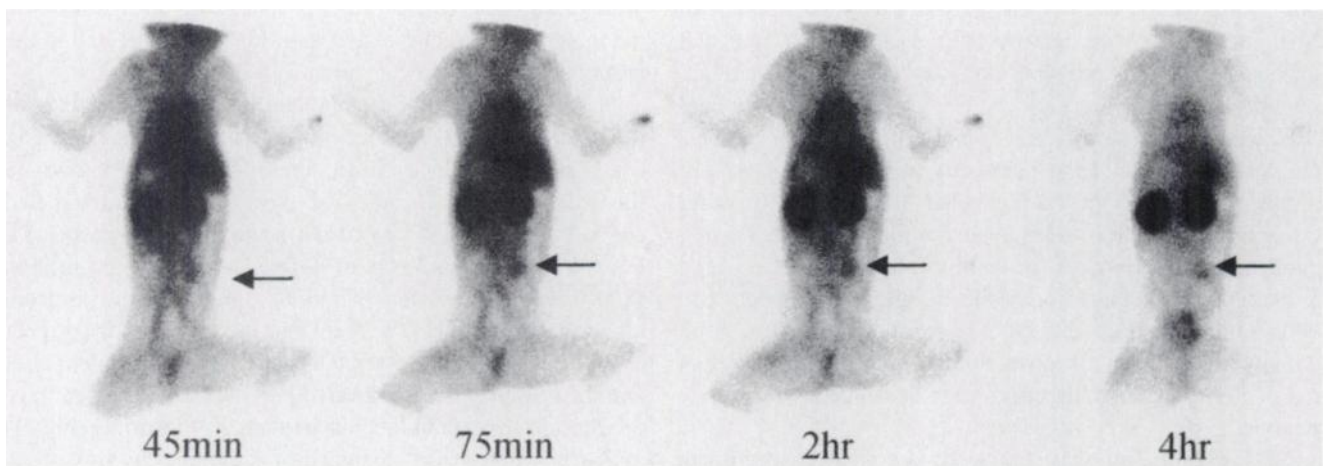


FIGURE 8. Series of whole-body images obtained between 45 min and 4 h postadministration of radiolabeled EPI-HNE-2 show radioactivity accumulations in kidneys, liver gallbladder, facial mucosa, heart, muscle, and nonsterile inflammatory lesion (arrows).

related proteases (18,19). The peptide used in these studies, EPI-HNE-2, differs from BPTI at only 8 of 58 homologous positions (18), shows high affinity and specificity for hNE, and is in the size range (mol wt = 6753 Da) expected to show rapid kinetics of localization and clearance.

The use of NHS-MAG₃ to attach ^{99m}Tc to EPI-HNE-2 appears to provide a suitable radiolabel. It had earlier been shown that this method provides a stable, high-specific-activity label when applied to this and other peptides (15). We have shown in this study that the attachment of 1 or more chelating groups onto EPI-HNE-2 and the mild reductive chemistry required to incorporate ^{99m}Tc into MAG₃ have no effect on the interaction of EPI-HNE-2 with hNE (Table 1).

As expected for a low molecular weight peptide, radiolabeled EPI-HNE-2 was found in this investigation to clear from plasma rapidly, such that the majority of administered radioactivity cleared from circulation in less than 30 min. Blood clearance shows biphasic kinetics (Fig. 2) and the observed blood $t_{1/2\alpha}$ and $t_{1/2\beta}$ times (7.3 min and 4 h, respectively) are similar to values obtained with other ^{99m}Tc-labeled peptides (35). Size-exclusion HPLC analysis of primate plasma samples taken after administration of labeled peptide (Fig. 2) shows that the decrease in blood radioactivity correlates with the disappearance of the ^{99m}Tc-MAG₃-EPI-HNE-2 elution peak. There is no evidence for the presence of low molecular weight ^{99m}Tc-labeled material (arising from peptide degradation or transchelation of label to cysteine) circulating in the blood at any time during the first 4 h postadministration.

A small high molecular weight peak, accounting for a few percent of the total radioactivity, appears in the earliest plasma samples analyzed and persists at about this initial level throughout the analysis period. We have shown that ^{99m}Tc-MAG₃-peptides incubated in vitro in human serum often provide a small high molecular weight peak on size-exclusion HPLC analysis (15). The formation of these high molecular weight peaks has been attributed to disulfide bond formation between the sulfur within the MAG₃ chelate and serum proteins (36). The high molecular weight peak is only partially removed from plasma after incubation with hNE immobilized on agarose (Fig. 1), demonstrating that this radioactivity is probably not associated with functional peptide.

The size-exclusion HPLC analysis of urine samples (Fig. 1) showed that the radioactivity therein was present almost exclusively as radiolabeled EPI-HNE-2 in early collections. At later times postadministration, increasing concentrations of what is probably ^{99m}Tc-cysteine resulting from in vivo transchelation of the radiolabel from peptide to endogenous cysteine (23,28) are present. However, even when collected at 6.5 h postadministration, the majority of radioactivity present in urine was associated with active peptide.

This investigation was conducted in a nonhuman primate model, because EPI-HNE-2 is expected to show low affinities for neutrophil elastase from nonprimates (A. C. Ley,

unpublished observations). The inflammation was induced with arachidonic acid and, occasionally, zymosan, 2 agents that have previously been used to induce inflammatory lesions in nonprimates (25–27). Live and heat-killed *S. aureus* were coadministered to augment the lesion. No obvious differences in the images were apparent between sterile and infected inflammations, and lesions were detectable within 24 h of induction in all cases. A pus-like exudate, obtained on lancing a lesion, was observed to contain abundant neutrophils. Tissue samples were removed for histology from both sterile and infected inflammations, and the infiltration of abundant neutrophils was discernible in all slides.

All images obtained with ^{99m}Tc-MAG₃-EPI-HNE-2 showed specific accumulation of radioactivity at the site of inflammation. The images shown in Figure 8 are representative of those obtained in this study. Radiolabel rapidly accumulates at the site of inflammation and remains associated with the site even though circulating levels of radioactivity have greatly diminished.

Because some degree of nonspecific accumulation within the inflammation is expected, especially at early time points, 2 sets of studies were conducted to establish nonspecific accumulation levels. The factor most likely to affect such penetration and subsequent nonspecific retention is molecular size. BPTI, which is about the same size as EPI-HNE-2, was selected for use as a nonbinding control peptide. To judge from images obtained using radiolabeled BPTI (Fig. 4), the extent of nonspecific accumulation and retention of small peptides at the inflammatory locus is minimal. Further, suppression of specific binding by predosing with a large excess of unlabeled EPI-HNE-2 results in the decrease of radioactivity in the lesion-to-background levels (Figs. 5 and 6).

We conclude from these results that the positive images of Figure 8 are the result of specific uptake of radiolabeled EPI-HNE-2 on monkey neutrophil elastase within the inflammatory site. It is particularly encouraging that positive images were obtained in the lower abdomen, where background radioactivity may be expected to adversely influence the images to a greater extent than for lesions located in the arm or shoulder (data not shown).

In addition to the site of inflammation, accumulation of radioactivity is apparent in kidneys and, to a lesser extent, liver and gallbladder. Since, these organs are known to represent the major routes of clearance for radiolabeled compounds (13,35,37–38), such accumulation is expected. For small peptides such as EPI-HNE-2, glomerular filtration in the kidneys is often the main route of removal from circulation (35,37–38) and so may account for the higher level of radiolabel associated with renal clearance after administration of ^{99m}Tc-MAG₃-EPI-HNE-2. The appearance of intact, active radiolabeled peptide in the urine (Fig. 1) indicates whole-body clearance of radiolabel by this route. Reabsorption of radiolabeled peptide in proximal renal tubules and subsequent catabolism (37) may account for the

continued accumulation of counts in kidney tissue (Fig. 3) and the appearance of low molecular weight radiolabeled material in the urine at later times.

Images obtained with radiolabeled nonspecific antibody were also of diagnostic quality in this investigation, as shown in Figure 7. Except for kidneys, background radioactivity levels were generally higher with the labeled antibody relative to labeled EPI-HNE-2, as expected.

The physical properties of ^{99m}Tc -labeled EPI-HNE-2 and IgG are reflected in accumulation at the inflammation. Accumulation of labeled EPI-HNE-2 is rapid but ceases after about 30 min postadministration (Fig. 3), presumably because of the equally rapid blood clearance. Despite low circulating levels of ^{99m}Tc -MAG₃-EPI-HNE-2 at longer times, radioactivity levels in the lesion remain unchanged (or increase somewhat) throughout the 4-h postadministration measurement period. In contrast, labeled IgG levels in the lesions are at first low and steadily increase. The lower initial levels reflect the slower diffusion to the site by the larger molecule, but lack of blood clearance allows accumulation throughout the measurement period so that after a few hours absolute levels of radioactivity are actually somewhat higher for IgG than for the peptide. The specific activities of the radiolabeled antibody administered were much greater than those of the radiolabeled EPI-HNE-2 peptide (approximately 3 versus 0.4 Ci/ μmol [i.e., 60 versus 20 $\mu\text{Ci}/\mu\text{g}$], respectively). Thus, a greater accumulation of radioactivity in the lesion will be accomplished by fewer molecules for labeled IgG than for labeled EPI-HNE-2. The somewhat higher levels of radioactivity in the lesion achieved with labeled antibody are likely to be offset by the higher levels in normal tissues, particularly for lesions located in the chest or upper abdomen. However, although the mechanism of localization of radiolabeled EPI-HNE-2 in inflammatory sites is to be specific to lesions infiltrated with activated neutrophils, the mechanism of localization of radiolabeled antibody is unknown (4).

Along with radiolabeled white blood cells, radiolabeled nonspecific antibodies are often considered the agent of choice for infection/inflammation imaging (5). To judge by the results of this and numerous other investigations, radiolabeled antibodies are unquestionably useful agents. However, as was also made clear in this research, background radioactivity levels will in general be higher with labeled antibodies relative to labeled EPI-HNE-2 and other peptides, especially in the chest and upper abdomen, where radioactivity in liver and blood pool of the heart can interfere. In the monkey inflammation model used in this investigation, somewhat greater accumulation of labeled antibody occurred in the lesion as well. It is possible that radiolabeled antibody shows superior sensitivity at the expense of specificity if localization, unlike that of EPI-HNE-2, is nonspecific. Further investigations in other infection/inflammation models are needed.

CONCLUSION

The hNE-specific inhibitor peptide EPI-HNE-2 can be radiolabeled with ^{99m}Tc by NHS-MAG₃ without loss of affinity, and the ^{99m}Tc -MAG₃-EPI-HNE-2 is not degraded in serum and shows radiochemical stability for an extended period of time in vivo. The labeled peptide was shown in a monkey model to localize rapidly and specifically in sites of inflammation. Radioactivity was present in normal tissues, in particular the kidneys, at levels that could interfere with localizing infection/inflammation in certain sites. Nevertheless, images of diagnostic quality were obtained within 20–40 min postadministration in all studies, including those in which the lesion was located within the lower abdomen.

ACKNOWLEDGMENTS

The authors thank M. Previti for help in the animal studies. Partial financial support for this investigation was provided by Dyax Corporation, Cambridge, MA, and by Grant R43-AI39340 from the National Institutes of Health.

REFERENCES

1. Lavander JP, Lowe J, Baker JR, Burns JI, Chaudri MA. Gallium-67 citrate scanning in neoplastic and inflammatory lesions. *Br J Rad.* 1971;44:361–366.
2. McAfee JG, Thakur ML. Survey of radioactive agents for the in vitro labeling of phagocytic leucocytes. I. Soluble agents. II. Particles. *J Nucl Med.* 1976;17:480–492.
3. Locher JT, Seybold K, Andres RY, et al. Imaging of inflammatory and infectious lesions after injection of radioiodinated monoclonal antigranulocyte antibodies. *Nucl Med Commun.* 1986;7:659–670.
4. Rubin RH, Young LS, Hansen WP, et al. Specific and nonspecific imaging of localized fisher immunotype 1 pseudomonas aeruginosa infection with radiolabeled monoclonal antibody. *J Nucl Med.* 1988;29:651–656.
5. Buscombe JR, Lui D, Ensing G, de Jong R, Eil PJ. ^{99m}Tc -human immunoglobulin (HIG)—first results of a new agent for the localization of infection and inflammation. *Eur J Nucl Med.* 1990;16:649–655.
6. Winker KH, Reuland P, Bihl H. Infektionsdiagnostik am skelettsystem mit Tc-99m-markierten nanocolloiden. *Nucl Compact.* 1989;20:219–223.
7. Fishman AJ, Pike MC, Kroon D, et al. Imaging focal sites of bacterial infection in rats with indium-111-labeled chemotactic peptide analogs. *J Nucl Med.* 1991;2:483–491.
8. Ruscowski M, Fritz B, Hnatowich DJ. Localization of infection using streptavidin and biotin: an alternative to nonspecific polyclonal immunoglobulin. *J Nucl Med.* 1992;33:1810–1815.
9. Babich J, Graham W, Barrow S, et al. Technetium-99m-labeled chemotactic peptides: comparison with indium-111-labeled white blood cells for localizing acute bacterial infection in the rabbit. *J Nucl Med.* 1993;34:2176–2184.
10. Vinjamuri S, Hall AV, Solanki KK, et al. Comparison of ^{99m}Tc -infecton with radiolabelled white cell imaging in the evaluation of bacterial infection. *Lancet.* 1996;347:233–235.
11. Thakur ML, Marcus CS, Henneman P, et al. Imaging inflammatory diseases with neutrophil-specific technetium-99m-labeled monoclonal antibody anti-SSEA-1. *J Nucl Med.* 1996;37:1789–1795.
12. Boerman OC, Oyen WJG, van Bloois L, et al. Optimization of technetium-99m-labeled PEG liposomes to image focal infections: effects of particle size and circulation time. *J Nucl Med.* 1997;38:489–493.
13. Chianelli M, Mather SJ, Martin-Comin J, Signore A. Radiopharmaceuticals for the study of inflammatory processes: a review. *Nucl Med Commun.* 1997;18:437–455.
14. Peters AM. The use of nuclear medicine in infections. *Br J Rad.* 1998;71:252–261.
15. Hnatowich DJ, Qu T, Chang F, Ley AC, Ladner RC, Ruscowski M. Labeling peptides with ^{99m}Tc using an NHS-MAG₃ bifunctional chelator. *J Nucl Med.* 1998;39:56–64.
16. Hallett MB. The significance of stimulus-response coupling in the neutrophil for physiology and pathology. In: Hallett MB, ed. *The Neutrophil: Cellular Biochemistry and Physiology*. Baton Rouge, FL: CRC Press; 1989:1–22.

17. Bieth JG. Human neutrophil elastase. In: Ladislav R, Hornebeck W, eds. *Elastin and Elastases*. Vol II. Boca Raton, FL: CRC Press; 1989:23–31.
18. Roberts BL, Markland W, Ley AC, et al. Directed evolution of a protein: selection of potent neutrophil elastase inhibitors displayed on M13 fusion phage. *Proc Natl Acad Sci USA*. 1992;89:2429–2433.
19. Ley AC, Ladner RC, Guterman SK, Roberts BL, Markland W, Kent RB, inventors. Engineered Human-Derived Kunitz Domains that Inhibit Human Neutrophil Elastase. US Patent 5,663,143. 1997.
20. Charlton J, Sennello J, Smith D. In vivo imaging of inflammation using an aptamer inhibitor of human neutrophil elastase. *Chem Biol*. 1997;4:809–816.
21. Winnard P Jr, Chang F, Rusckowski M, Mardirossian G, Hnatowich DJ. Preparation and use of NHS-MAG₃ for technetium-99m labeling of DNA. *Nucl Med Biol*. 1997;24:425–432.
22. Schwarz A, Steinstrasser A. A novel approach to Tc-99m labeling of murine monoclonal antibody fragments [abstract]. *J Nucl Med*. 1987;28:721.
23. Hnatowich DJ, Virzi F, Fogarasi M, Winnard P Jr, Rusckowski M. Can a cysteine challenge assay predict the in vivo behavior of ^{99m}Tc-labeled to antibodies? *Nucl Med Biol*. 1994;21:1035–1044.
24. Lei K, Rusckowski M, Chang F, Qu T, Mardirossian G, Hnatowich DJ. Technetium-99m antibodies labeled with MAG₃ and SHNH—an in vitro and animal in vivo comparison. *Nucl Med Biol*. 1996;23:917–922.
25. Kikuchi M, Tsuzurahara K, Naito K. Involvement of leukotriene B₄ in zymosan-induced rat pleurisy: inhibition of leukocyte infiltration by the 5-lipoxygenase inhibitor T-0757. *Biol Pharm Bull*. 1995;19:1302–1304.
26. Samuelsson B, Dahlén S-E, Lindren JÅ, Rouzer CA, Serhan CN. Leukotrienes and lipoxins: structures, biosynthesis, and biological effects. *Science*. 1987;237:1171–1176.
27. Van der Laken CJ, Boerman OC, Oyen WJG, et al. Technetium-99m-labeled chemotactic peptides in acute infection and sterile inflammation. *J Nucl Med*. 1997;38:1310–1315.
28. Mardirossian G, Wu C, Rusckowski M, Hnatowich DJ. The stability of technetium-99m directly labeled to an Fab' antibody via stannous ion and mercaptoethanol reduction. *Nucl Med Commun*. 1992;13:503–512.
29. Bourne DWA. Boomer: a simulation and modeling program for pharmacokinetic and pharmacodynamic data analysis. *Comput Methods Programs Biomed*. 1989;29:191–195.
30. Babich JW, Tompkins RG, Graham W, Barrow SA, Fischman AJ. Localization of radiolabeled chemotactic peptide at focal sites of *Escherichia coli* infection in rabbits: evidence for a receptor-specific mechanism. *J Nucl Med*. 1997;38:1316–1322.
31. Babich JW, Solomon H, Oike MC, et al. Technetium-99m-labeled hydrazino nicotinamide derivatized chemotactic peptide analogs for imaging focal sites of bacterial infection. *J Nucl Med*. 1993;34:1964–1974.
32. Pollak A, Goodbody AE, Ballinger JR, et al. Imaging inflammation with ^{99m}Tc-labeled chemotactic peptides: analogues with reduced neutropenia. *Nucl Med Commun*. 1996;17:132–139.
33. Hallett MB. The significance of stimulus-response coupling in the neutrophil for physiology and pathology. In: Hallett MB, ed. *The Neutrophil: Cellular Biochemistry and Physiology*. Boca Raton, FL: CRC Press; 1989: Chapter 1.
34. Salvesen G, Travis J. Properties of naturally occurring elastase inhibitors. In: Ladislav R, Hornebeck W, eds. *Elastin and Elastases*. Vol II. Boca Raton, FL: CRC Press; 1989: Chapter 11.
35. Lister-James J, Moyer BJ, Dean TR. Pharmacokinetic considerations in the development of peptide-based imaging agents. *Quart J Nucl Med*. 1997;41:111–118.
36. Hnatowich DJ, Chang F, Qu T, Rusckowski M. Technetium-99m labeled peptides—an investigation of multiple HPLC peaks. *Appl Radiat Isot*. 1999;50:911–921.
37. Rutherford RAD, Smith A, Waibel R, Shubiger PA. Differential inhibitory effect of L-lysine on renal accumulation of ⁶⁷Cu-labelled F(ab')₂ fragments in mice. *Int J Cancer*. 1997;72:522–529.
38. Yoo TM, Chang HK, Choi CW, et al. Technetium-99m labeling and biodistribution of anti-TAC disulfide-stabilized Fv fragment. *J Nucl Med*. 1997;38:294–300.